



Intravoxel incoherent motion diffusion-weighted MRI for the characterization of inflammation in chronic liver disease

Thierry Lefebvre^{1,2,3} · Mélanie Hébert^{1,2} · Laurent Bilodeau^{1,2} · Giada Sebastiani⁴ · Milena Cerny^{1,2} · Damien Olivé¹ · Zu-Hua Gao⁵ · Marie-Pierre Sylvestre^{2,6} · Guy Cloutier^{1,7,8} · Bich N. Nguyen⁹ · Guillaume Gilbert^{1,10} · An Tang^{1,2,7} 

Received: 28 March 2020 / Revised: 10 June 2020 / Accepted: 18 August 2020 / Published online: 2 September 2020
© European Society of Radiology 2020

Abstract

Objective To evaluate the diagnostic performance of intravoxel incoherent motion (IVIM) diffusion-weighted imaging (DWI) for grading hepatic inflammation.

Methods In this retrospective cross-sectional dual-center study, 91 patients with chronic liver disease were recruited between September 2014 and September 2018. Patients underwent 3.0-T MRI examinations within 6 weeks from a liver biopsy. IVIM parameters, perfusion fraction (f), diffusion coefficient (D), and pseudo-diffusion coefficient (D^*), were estimated using a voxel-wise nonlinear regression on DWI series (10 b -values from 0 to 800 s/mm²). The reference standard was histopathological analysis of hepatic inflammation grade, steatosis grade, and fibrosis stage. Intraclass correlation coefficients (ICC), univariate and multivariate correlation analyses, and areas under receiver operating characteristic curves (AUC) were assessed.

Results Parameters f , D , and D^* had ICCs of 0.860, 0.839, and 0.916, respectively. Correlations of f , D , and D^* with inflammation grade were $\rho = -0.70$, $p < 0.0001$; $\rho = 0.10$, $p = 0.35$; and $\rho = -0.27$, $p = 0.010$, respectively. When adjusting for fibrosis and steatosis, the correlation between f and inflammation ($p < 0.0001$) remained, and that between f and fibrosis was also significant to a lesser extent ($p = 0.002$). AUCs of f , D , and D^* for distinguishing inflammation grades 0 vs. ≥ 1 were 0.84, 0.53, and 0.70; ≤ 1 vs. ≥ 2 were 0.88, 0.57, and 0.60; and ≤ 2 vs. 3 were 0.86, 0.54, and 0.65, respectively.

Conclusion Perfusion fraction f strongly correlated, D very weakly correlated, and D^* weakly correlated with inflammation. Among all IVIM parameters, f accurately graded inflammation and showed promise as a biomarker of hepatic inflammation.

Key Points

- IVIM parameters derived from DWI series with 10 b -values are reproducible for liver tissue characterization.
- This retrospective two-center study showed that perfusion fraction provided good diagnostic performance for distinguishing dichotomized grades of inflammation.
- Fibrosis is a significant confounder on the association between inflammation and perfusion fraction.

Electronic supplementary material The online version of this article (<https://doi.org/10.1007/s00330-020-07203-y>) contains supplementary material, which is available to authorized users.

✉ An Tang
an.tang@umontreal.ca

¹ Department of Radiology, Radio-Oncology and Nuclear Medicine, Université de Montréal, Montréal, Canada

² Centre de recherche du Centre hospitalier de l'Université de Montréal (CRCHUM), Montréal, Canada

³ Medical Physics Unit, McGill University, Montréal, Canada

⁴ Division of Gastroenterology and Hepatology, Department of Medicine, McGill University Health Centre (MUHC), Montréal, Canada

⁵ Department of Pathology, McGill University, Montréal, Canada

⁶ Department of Social and Preventive Medicine, École de santé publique de l'Université de Montréal (ESPUM), Montréal, Canada

⁷ Institute of Biomedical Engineering, Université de Montréal, Montréal, Canada

⁸ Laboratory of Biorheology and Medical Ultrasonics (LBUM), Centre de recherche du Centre hospitalier de l'Université de Montréal (CRCHUM), Montréal, Canada

⁹ Service of Pathology, Centre hospitalier de l'Université de Montréal (CHUM), Montréal, Canada

¹⁰ MR Clinical Science, Philips Healthcare Canada, Markham, Canada

Keywords Inflammation · Diffusion-weighted MRI · Biopsy · Hepatitis · Nonalcoholic fatty liver disease

Abbreviations

ADC	Apparent diffusion coefficient
AIH	Autoimmune hepatitis
AUC	Area under the ROC curve
CI	Confidence interval
CLD	Chronic liver disease
DWI	Diffusion-weighted imaging
HBV	Hepatitis B virus
HCV	Hepatitis C virus
ICC	Intraclass correlation coefficient
IVIM DWI	Intravoxel incoherent motion diffusion-weighted imaging
MRI	Magnetic resonance imaging
NAFLD	Nonalcoholic fatty liver disease
NASH CRN	NASH Clinical Research Network
NASH	Nonalcoholic steatohepatitis
NPV	Negative predictive value
PDFF	Proton density fat fraction
PPV	Positive predictive value
ROC	Receiver operating characteristic
SPIR	Spectral presaturation inversion recovery

Introduction

Chronic liver disease (CLD) describes a spectrum of long-term liver disease caused by viral, metabolic, toxic, or autoimmune causes that carry an important economic and clinical burden on healthcare systems. The most prevalent condition, nonalcoholic fatty liver disease (NAFLD), costs upwards of \$100 billion annually in the USA [1]. Given this disease spectrum, CLD has several histopathological manifestations, including lobular inflammation, hepatocyte ballooning, steatosis, and fibrosis [2]. Inflammation constitutes a manifestation of disease activity and may lead to stellate cell activation, liver fibrosis [3], and cirrhosis [4, 5]. The presence of inflammation and ballooning characterizes nonalcoholic steatohepatitis (NASH), the progressive form of NAFLD, and is found in other conditions such as viral hepatitis and autoimmune hepatitis. Noninvasive detection and grading of inflammation are critical for early characterization of CLD.

Diffusion-weighted imaging (DWI) was previously proposed as a noninvasive technique for staging liver fibrosis through detection of diffusion- and perfusion-related changes [6, 7]. Earlier works have proposed a mono-exponential approach for estimating the apparent diffusion coefficient (ADC) [8–10]. Recent reports favor a bi-exponential approach to fit nonlinearly intravoxel incoherent motion (IVIM) DWI parameters, such as the perfusion fraction (f), the diffusion coefficient (D), and the pseudo-diffusion coefficient (D^*)

[11–13]. IVIM DWI assesses diffusion and perfusion in image voxels at the microcirculation level by capturing random movements of water molecules [14]. Most studies included heterogeneous cohorts of CLD [6, 7, 12, 13], although a few studies have targeted NAFLD [15, 16], viral hepatitis B [17, 18], and viral hepatitis C [8, 19].

In the last decade, two experimental animal studies have observed that f decreases in the presence of inflammation in animal models with NAFLD or NASH [20, 21]. Both studies demonstrated the diagnostic value of f to distinguish NAFLD from NASH and one also showed that f could distinguish advanced inflammation from moderate or negligible inflammation. Since the onset of inflammation predicts the progression of fibrosis and disease activity [22], noninvasive detection and grading of inflammation are urgently needed. Because histopathological features of CLD such as steatosis, inflammation, and fibrosis may co-exist, the impact of these confounders on IVIM parameters must also be assessed.

The purpose of this study was to evaluate the diagnostic performance of IVIM parameters for assessing histology-determined inflammation grades in patients with CLD. The secondary aims were to evaluate the confounding effects of other histopathological features (i.e., steatosis and fibrosis) and to compare IVIM parameters and proton density fat fractions (PDFF) in subgroups with inflammatory or fatty liver diseases.

Materials and methods

Study design and patients

This is a retrospective, cross-sectional ancillary study to a diagnostic clinical trial (ClinicalTrials.gov identifier no. NCT02044523). Study protocol was approved by the Institutional Review Board of the two participating institutions. All patients provided written informed consent. The prior prospective cross-sectional trial provided paired comparisons of ultrasound- and magnetic resonance-based elastography for staging liver fibrosis [23].

In this ancillary study, IVIM DWI sequences were analyzed to evaluate their diagnostic performance in assessing histology-determined inflammation. MRI examinations were performed within 6 weeks of the liver biopsy with a minimal delay of 48 h if performed after the biopsy.

The hepatology clinics of both institutions recruited participants between September 2014 and September 2018. Adult patients who underwent a liver biopsy as part of their clinical standard of care for suspected or known CLD caused by

hepatitis B virus (HBV), hepatitis C virus (HCV), NAFLD, NASH, autoimmune hepatitis (AIH), or mixed etiologies were included. Candidates with liver biopsies to distinguish between fibrosis stages inferred by FibroScan and by noninvasive laboratory scoring systems were also included. Patients were excluded if MRI was contra-indicated or if they were unable to provide written informed consent.

MRI examinations

Eligible patients were examined in supine position in a fasted state with a clinical 3.0-T scanner (Achieva TX; Philips Healthcare) using a 16-channel body array for signal reception. IVIM DWI was performed using a respiratory-triggered spin-echo diffusion-weighted echoplanar imaging sequence. Since fat confounds DWI signals [24], combined spectral presaturation inversion recovery (SPIR) and gradient reversal were used to remove fat signal from the DWI acquisition [25]. DWI was acquired at 10 b -values (0, 10, 20, 30, 40, 50, 100, 200, 400, 800 s/mm²). Total acquisition time was about 6 min, depending on breathing. MRI PDFF was acquired with a seven-echo spoiled gradient-echo sequence of the whole liver during a single breath-hold. Echoes were acquired using a bipolar readout scheme within a single TR. Sequence parameters are detailed in Supplementary Table 1.

MRI post-processing

IVIM DWI parameters (perfusion fraction— f ; true diffusion coefficient— D , and pseudo-diffusion coefficient— D^*) were obtained using a least squares nonlinear regression on a segmented bi-exponential model on DWI signals (SI) at different b -values (equation below) using MATLAB R2018a (MathWorks).

$$\frac{SI(b)}{SI(b = 0 \text{ s/mm}^2)} = (1-f)e^{-bD} + fe^{-bD^*}$$

Fast perfusion components, f and D^* associated with the fraction of flowing blood and the velocity of capillary blood, respectively, were obtained on the first part of DWI series ($b < 150$ s/mm²). The slow diffusion component, D associated with tissue molecular diffusion, was evaluated on the later part of DWI series ($b > 150$ s/mm²) (Fig. 1) [26]. Apparent diffusion coefficient (ADC) values were also obtained using three b -values (100, 400, and 800 s/mm²) excluding $b = 0$ s/mm² to remove perfusion effects, according to a recent consensus [27].

A region of interest (ROI) encompassing the liver over 5 central axial slices located at least 2.5 cm below the dome of the diaphragm was used. A radiology resident (L.B., 3 years of

experience in liver MRI) supervised by an experienced abdominal radiologist (A.T., 14 years of experience in liver MRI) manually selected these sequential transverse slices and segmented the liver parenchyma on images with $b = 0$ s/mm². All images were registered to the $b = 0$ s/mm² image using a nonrigid motion correction algorithm [28]. Voxels with $f > 0.5$ were discarded from the calculation as they belonged to large vessels. In fact, average f in segmented vessels in randomly sampled patients ($n = 30$) was 0.48 ± 0.08 (mean \pm standard deviation). Only series of voxels for which the normalized root mean squared error (NRMSE) of the regression was lower than 0.05 were included in calculation, to account for residual breathing and cardiac motion. A fellowship-trained abdominal radiologist (M.C., 4 years of experience in liver MRI) repeated segmentation in the subgroup ($n = 30$) to evaluate inter-reader variability of IVIM parameters. The second reader also performed another segmentation manually excluding large vessels (i.e., portal vein and inferior vena cava) on the same 5 slices and IVIM parameters were re-evaluated to assess bias induced by the f threshold used.

Similarly, PDFF maps were obtained using a voxel-wise nonlinear least squares fitting based on all echoes according to previously reported methodologies [29, 30]. Reported mean PDFF values were calculated from 5 axial slices.

Histopathological analysis

Histopathological features were centrally analyzed by a liver pathologist (B.N.N., 21 years of experience in hepatopathology). Sixteen- to 18-gauge percutaneous ultrasound-guided liver biopsies were performed in the right lobe. Liver biopsies were fixed in formalin 10% and processed according to clinical standard of care. Paraffin sections were stained with hematoxylin and eosin, Masson's trichrome, periodic acid-Schiff-diastase, reticulin, and Perls' Prussian blue for iron staining in all cases. For patients with HBV, HCV, or AIH ($n = 37$), the METAVIR scoring system was used to grade inflammatory activity from 0 to 3 and fibrosis stages from F0 to F4. For patients with NAFLD or NASH ($n = 47$), the NASH Clinical Research Network (NASH CRN) scoring system was used to grade lobular inflammation from 0 to 3 and fibrosis from F0 to F4 [31, 32]. Steatosis grading for all cases was performed on an ordinal scale from 0 to 3 by assessing proportion of hepatocytes with macrovesicles of fat. Inflammation grades throughout this study refer to inflammatory activity grades and lobular inflammation grades as scored by the METAVIR and the NASH CRN scoring systems, respectively. Biopsy specimens from patients with mixed CLD causes were assessed using the scoring system associated with the dominant cause of CLD ($n = 7$).

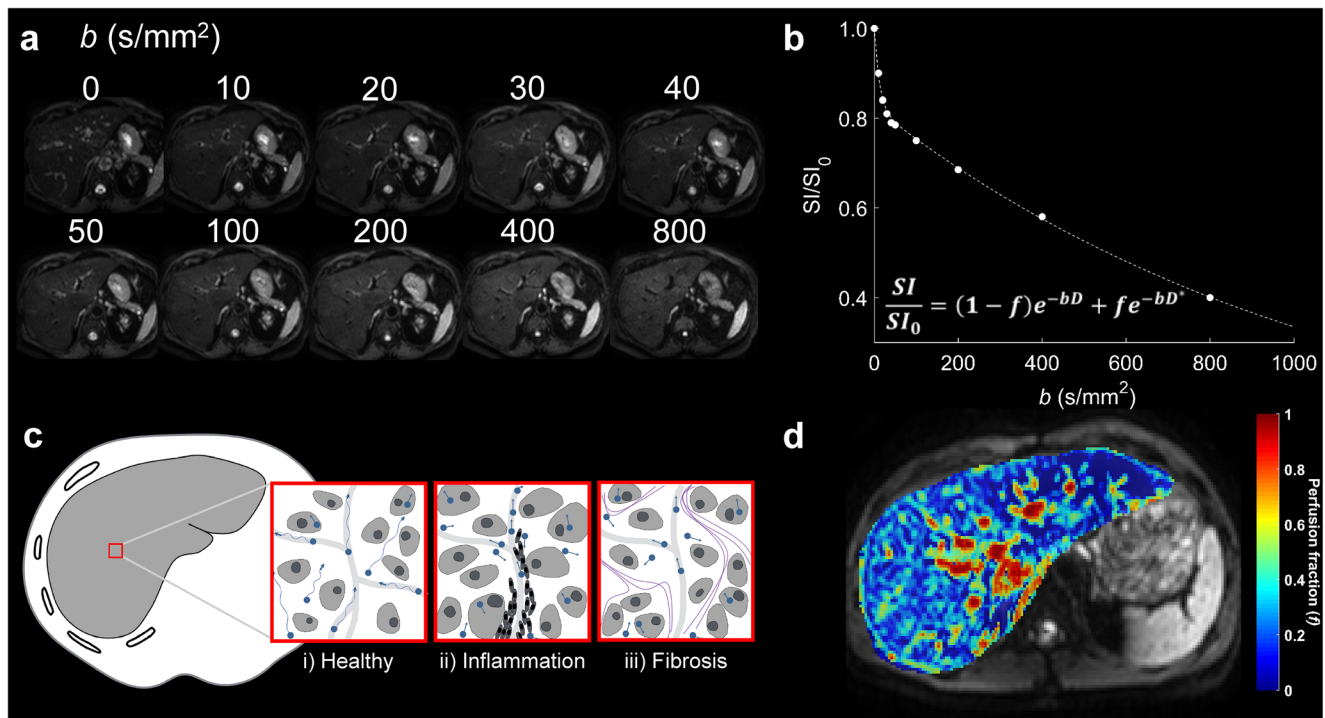


Fig. 1 Schematic of intravoxel incoherent motion diffusion-weighted imaging. **a** Diffusion-weighted image series are used to fit **(b)** signal intensities in each voxel with a nonlinear regression on a segmented bi-exponential model. **c** Water diffusion schematic shows altered molecule

diffusion associated with histopathological changes in liver disease. **d** Perfusion fraction map (color) extracted from diffusion-weighted series shows the distribution of the perfusion component in the intravoxel incoherent motion model

Blinding

The pathologist was blinded to imaging results. The image analysts were blinded to the biopsy results.

Statistical analysis

Statistical analyses were supervised by a senior biostatistician with SPSS 25 (SPSS Statistics) and the open-source software R 3.4.2 (R Foundation). Statistical significance was defined after Bonferroni correction as $p < 0.01$ to account for multiple comparisons between pairs of IVIM parameters and histopathological features. Normality of variables was tested using the Shapiro-Wilk test. Non-normally distributed variables were compared using non-parametric tests.

Inter-reader variability Intraclass correlation coefficients (ICC) were reported to assess the inter-reader variability of IVIM parameters in a randomly sampled subgroup ($n = 30$) [33]. The agreement of measurements was considered poor ($ICC < 0.50$), good ($0.50 \leq ICC < 0.80$), very good ($0.80 \leq ICC < 0.90$), or excellent ($ICC \geq 0.90$).

Correlation analysis Estimates of Spearman's ρ were used to assess correlations between histopathological features and index tests. Rank correlations were considered negligible ($|\rho| < 0.10$), weak ($0.10 \leq |\rho| < 0.40$), moderate

($0.40 \leq |\rho| < 0.70$), strong ($0.70 \leq |\rho| < 0.90$), or very strong ($|\rho| \geq 0.90$) [34]. Multiple regression analyses were performed to assess associations when more than one significant correlation was found on univariate analysis. Estimated regression coefficients, standard deviation of coefficients, standardized regression coefficients, and adjusted R^2 of regression models without interaction effects were reported.

Grading comparison Differences of index test measurements across all histopathological feature grades were tested using the nonparametric Kruskal-Wallis rank sum test. Pairwise comparisons of index tests were performed between grades of histopathological features with a post hoc Mann-Whitney U test with Bonferroni correction.

Diagnostic performance The diagnostic performance of IVIM parameters for grading hepatic inflammation was assessed using receiver operating characteristic (ROC) analyses to compute areas under the ROC curve (AUC). Thresholds maximizing Youden's index were identified and associated sensitivities, specificities, accuracies, positive predictive values (PPV), and negative predictive values (NPV) were reported. Bootstrapping was used to evaluate 95% confidence intervals (CI) of each diagnostic performance metric by resampling measurements 2000 times. AUCs were compared using the DeLong method [35].

Subgroup analysis Differences of index tests measurements within subgroups were explored. The cohort was divided based on the etiology of CLD, notably inflammatory causes (i.e., HBV, HCV, or AIH) and fatty liver disease (i.e., NAFLD or NASH). Differences were also explored across grades of histopathological features in these subgroups.

Results

Ninety-one eligible patients were included in the final cohort (Fig. 2). Patients’ mean age was 56 ± 12 years (range: 23–79 years) and 44 were women (48%) (Table 1). All patients had suspected or known liver fibrosis induced by either HBV (3 of 91, 3%), HCV (20 of 91, 22%), NAFLD (5 of 91, 6%), NASH (42 of 91, 46%), AIH (14 of 91, 15%), or mixed etiology (7 of 91, 8%).

Inflammation grades 0, 1, 2, and 3 were found in 8 (9%), 46 (50%), 28 (31%), and 9 (10%) patients, respectively. Steatosis grades 0, 1, 2, and 3 were found in 33 (36%), 25 (27%), 15 (17%), and 18 (20%) patients, respectively. Fibrosis stage F0, F1, F2, F3, and F4 were found in 14 (15%), 15 (17%), 23 (25%), 16 (18%), and 23 (25%) patients, respectively. The interval of time between the MRI and the biopsy was 24 ± 10 days on average (range: 1 day–6 weeks).

Perfusion fraction (*f*) was 0.25 ± 0.04 (mean ± standard deviation) (range: 0.17–0.33); true diffusion coefficient (*D*) was 0.97 ± 0.18 × 10⁻³ mm²/s (0.63 × 10⁻³–1.35 × 10⁻³ mm²/s); pseudo-diffusion coefficient (*D**) was 59.7 ± 14.0 × 10⁻³ mm²/s (34.3 × 10⁻³–108.6 × 10⁻³ mm²/s); mean ADC was 0.99 ± 0.17 × 10⁻³ mm²/s (0.62 × 10⁻³–1.43 × 10⁻³ mm²/s); and mean PDFF was 12.1 ± 9.9% (1.2–43.6%) (Table 2). These values were calculated in ROIs of 623.8 ± 199.9 cm² on average (239.2–999.5 cm²).

Inter-reader variability

In the subset of patients with segmentations by two readers (*n* = 30), the ICC was 0.860 for *f*, 0.839 for *D*, 0.916 for *D**, and 0.911 for ADC. When manually excluding large vessels and without using a *f* threshold of 0.5 in the same subset of patients, ICC was reduced to 0.760 for *f*, 0.513 for *D*, 0.907 for *D**, and 0.886 for ADC.

Correlation analysis

In univariate analysis, correlations of *f*, *D*, and *D** with inflammation grades were ρ = -0.70, *p* < 0.0001; ρ = 0.10, *p* = 0.35; and ρ = -0.27, *p* = 0.010, respectively (Table 3, Fig. 3). Parameter *f* also showed a negative correlation with fibrosis (ρ = -0.46, *p* < 0.0001) and was positively correlated, to a lesser extent, with steatosis (ρ = 0.35, *p* = 0.001). *D*, ADC,

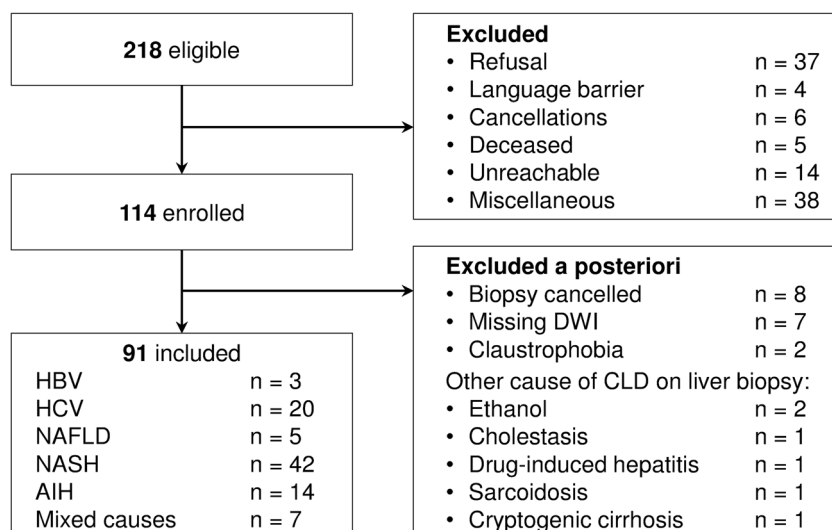
Table 1 Characteristics in 91 patients

Characteristic	Data
Sex	
Male	47 (52%)
Female	44 (48%)
Age (year)	
Mean ± SD (range)	56 ± 12 (23–79)
BMI (kg/m ²)	
Mean ± SD (range)	29.6 ± 5.9 (17–45)
< 25	20 (22%)
≥ 25 and < 30	26 (28%)
≥ 30 and < 40	41 (45%)
≥ 40	4 (5%)
Other medical conditions	
Diabetes	26 (28%)
Hypertension	35 (38%)
Laboratory tests: mean ± SD (range)	
AST (U/L)	57.8 ± 55.1 (14–319)
ALT (U/L)	77.4 ± 77.8 (13–473)
GGT (U/L)	79.9 ± 96.0 (11–464)
Platelet count (× 10 ⁹ /L)	205.6 ± 68.4 (78–383)
Total bilirubin (μmol/L)	12.8 ± 5.4 (4.5–29.0)
Prothrombin time (%)	100.1 ± 8.2 (83–120)
Alkaline phosphatase (U/L)	82.0 ± 46.2 (29–344)
Albumin (g/L)	40.9 ± 6.0 (31–79)
Cholesterol (mmol/L)	4.6 ± 1.0 (2.9–7.6)
Biopsy length (mm)	
Mean ± SD (range)	20.2 ± 6.1 (10–30)
Inflammation grade	
0 (none, no foci)	8 (9%)
1 (negligible, < 2 foci per 20× field)	46 (50%)
2 (moderate, 2–4 foci per 20× field)	28 (31%)
3 (severe, > 4 foci per 20× field)	9 (10%)
Fibrosis stage	
0 (none)	14 (15%)
1 (perisinusoidal or periportal)	15 (17%)
2 (periportal and presence of septa)	23 (25%)
3 (numerous septa without cirrhosis)	16 (18%)
4 (cirrhosis)	23 (25%)
Steatosis grade	
0 (< 5% hepatocytes involved)	33 (36%)
1 (5–33% hepatocytes involved)	25 (27%)
2 (33–66% hepatocytes involved)	15 (17%)
3 (> 66% hepatocytes involved)	18 (20%)

SD standard deviation, *BMI* body mass index, *AST* aspartate aminotransferase, *ALT* alanine aminotransferase, *GGT* gamma-glutamyl transpeptidase

and PDFF measurements were significantly correlated with histopathological steatosis grades (ρ = -0.34, *p* < 0.001; ρ = -0.25, *p* = 0.010; and ρ = 0.88, *p* < 0.0001; respectively).

Fig. 2 Flowchart of patient selection



A multiple regression analysis including inflammation, fibrosis, and steatosis grades was performed to assess which histopathological feature was most associated with f . In the multiple regression model, the correlation between f and inflammation remained ($p < 0.0001$), while the correlation with fibrosis decreased ($p = 0.002$), and the correlation with steatosis lost significance ($p = 0.075$) as reported in Table 3. Representative f maps in patients with different inflammation grades are shown in Fig. 4.

Grading comparison

Post hoc tests revealed that f values were significantly different between dichotomized groups of inflammation grades 0 vs. 1, 1 vs. 2, and 2 vs. 3 ($p < 0.01$). D , D^* , and ADC were not significantly different between any dichotomized groups of inflammation grades.

Diagnostic performance

Estimates of diagnostic performance of IVIM parameters and ADC for grading inflammation are shown in Table 4. For f , AUC was 0.84 (95% CI: 0.74–0.96) to distinguish inflammation grades 0 vs. ≥ 1 , 0.88 (0.82–0.95) for ≤ 1 vs. ≥ 2 , and 0.86 (0.78–0.96) for ≤ 2 vs. 3 (Table 4, Fig. 5). AUC of D was 0.53 (0.33–0.71) to distinguish inflammation grades 0 vs. ≥ 1 , 0.57 (0.45–0.69) for ≤ 1 vs. ≥ 2 , and 0.54 (0.31–0.77) for ≤ 2 vs. 3. AUC of D^* was 0.70 (0.51–0.90) to distinguish inflammation grades 0 vs. ≥ 1 , 0.60 (0.46–0.70) for ≤ 1 vs. ≥ 2 , and 0.65 (0.43–0.85) for ≤ 2 vs. 3.

Parameter f provided higher AUCs than D for distinguishing inflammation grades 0 vs. ≥ 1 (0.84 vs. 0.53, $p < 0.001$), ≤ 1 vs. ≥ 2 (0.88 vs. 0.57, $p < 0.0001$), and ≤ 2 vs. 3 (0.86 vs. 0.54, $p < 0.001$). Even if D^* values were also significantly correlated with inflammation grades, f provided higher

AUCs than D^* for distinguishing inflammation grades 0 vs. ≥ 1 (0.84 vs. 0.70, $p = 0.009$), ≤ 1 vs. ≥ 2 (0.88 vs. 0.60, $p < 0.0001$), and ≤ 2 vs. 3 (0.86 vs. 0.65, $p = 0.007$).

Subgroup analysis

To further assess the impact of fibrosis and inflammation on f , differences in f across fibrosis stages when separating groups with none to negligible inflammation (0–1) from moderate to severe inflammation (2–3) were explored and are shown in Fig. 6. Post hoc tests showed significant differences between paired groups of low inflammation and more advanced inflammation in patients with fibrosis stages F0, F1, and F4 ($p < 0.01$). ROC curves of f for staging liver fibrosis and for grading inflammation grades in each subgroup are shown in Supplemental Figure 1.

When separating subgroups of inflammatory (i.e., HBV, HCV, or AIH) and fatty liver diseases (i.e., NAFLD or NASH), f still correlated with inflammation grade in each subgroup ($\rho = -0.62$ and $\rho = -0.48$, respectively, $p < 0.0001$).

On average, patients with inflammatory liver disease had consistently lower f within a same inflammation grade and PDFF within a same steatosis grade than patients with fatty liver disease as shown in Fig. 6. However, post hoc tests revealed no significant f difference between paired groups of inflammation grades when separating the two disease subgroups. Only PDFF values were significantly different between subgroups for patients with steatosis grade 3 ($p < 0.01$).

Discussion

This retrospective clinical study evaluated IVIM parameters as biomarkers of inflammation by using histopathology as the

Table 2 Average IVIM parameters and ADC in patients with different histopathological feature grades

		Perfusion fraction (<i>f</i>)	True diffusion coefficient (<i>D</i> , 10 ⁻³ mm ² /s)	Pseudo-diffusion coefficient (<i>D*</i> , 10 ⁻³ mm ² /s)	Apparent diffusion coefficient (ADC, 10 ⁻³ mm ² /s)	
Inflammation grade	0	0.29 ± 0.02	0.95 ± 0.12	69.3 ± 14.1	0.96 ± 0.10	
		0.28 (0.27–0.29)	0.92 (0.90–1.04)	69.0 (57.6–78.6)	0.96 (0.89–1.01)	
	1	0.27 ± 0.03	0.95 ± 0.17	60.1 ± 14.8	0.97 ± 0.16	
		0.27 (0.25–0.28)	0.94 (0.82–1.10)	60.5 (57.6–68.6)	0.99 (0.83–1.10)	
	2	0.23 ± 0.02	0.99 ± 0.17	58.2 ± 12.1	1.01 ± 0.16	
		0.23 (0.22–0.26)	0.99 (0.84–1.08)	58.8 (52.4–64.3)	1.01 (0.89–1.07)	
	3	0.21 ± 0.02	1.04 ± 0.30	54.1 ± 13.4	1.06 ± 0.28	
		0.21 (0.20–0.23)	1.00 (0.83–1.11)	51.0 (46.9–60.8)	0.99 (0.89–1.11)	
	Steatosis grade	0	0.24 ± 0.03	1.05 ± 0.20	57.6 ± 13.6	1.07 ± 0.19
			0.23 (0.22–0.26)	1.03 (0.92–1.17)	58.3 (47.1–64.3)	1.04 (0.95–1.18)
		1	0.26 ± 0.03	0.92 ± 0.15	61.9 ± 15.2	0.93 ± 0.14
			0.26 (0.24–0.28)	0.91 (0.81–1.04)	61.7 (52.3–68.9)	0.95 (0.80–1.05)
2		0.26 ± 0.04	0.98 ± 0.14	61.8 ± 14.9	1.00 ± 0.13	
		0.26 (0.23–0.28)	0.96 (0.89–1.07)	57.3 (52.6–69.8)	1.00 (0.89–1.06)	
3		0.27 ± 0.02	0.90 ± 0.16	58.8 ± 12.7	0.93 ± 0.16	
		0.27 (0.26–0.27)	0.88 (0.78–1.04)	59.6 (52.6–65.0)	0.94 (0.81–1.04)	
Fibrosis stage		0	0.28 ± 0.03	1.00 ± 0.17	59.7 ± 15.8	1.01 ± 0.18
			0.28 (0.26–0.30)	1.02 (0.85–1.11)	58.5 (50.7–66.4)	1.03 (0.84–1.11)
		1	0.26 ± 0.03	1.04 ± 0.17	58.9 ± 15.1	1.05 ± 0.15
			0.27 (0.24–0.28)	1.09 (0.90–1.12)	55.5 (45.9–72.3)	1.07 (0.98–1.15)
	2	0.26 ± 0.02	0.95 ± 0.17	64.3 ± 15.2	0.98 ± 0.16	
		0.26 (0.24–0.28)	0.93 (0.83–1.06)	62.3 (56.3–71.3)	0.99 (0.86–1.07)	
	3	0.26 ± 0.03	0.92 ± 0.17	58.9 ± 12.7	0.94 ± 0.18	
		0.26 (0.25–0.27)	0.93 (0.79–1.03)	57.5 (51.0–66.0)	0.95 (0.79–1.06)	
	4	0.22 ± 0.03	0.98 ± 0.20	56.4 ± 11.7	0.99 ± 0.18	
		0.22 (0.21–0.25)	0.94 (0.86–1.02)	56.4 (49.0–61.2)	0.97 (0.89–1.04)	

Data are shown as mean ± standard deviation, median (interquartile range)

reference standard. We found that the inter-reader agreement was very good for perfusion fraction *f* and true diffusion coefficient *D*, and excellent for pseudo-diffusion coefficient *D** and ADC. The perfusion fraction *f* correlated strongly with inflammation grade, even when accounting for steatosis and fibrosis. Parameters *D* and *D** were very weakly and weakly correlated with inflammation grade, respectively. The correlation between steatosis grade and IVIM parameters or ADC was either weak or negligible. Furthermore, *f* differed significantly between all dichotomized inflammation grades and provided good classification accuracy to distinguish them. Finally, within each inflammation grade, *f* did not significantly differ between patients with NAFLD spectrum and inflammatory diseases. The only difference between disease categories was higher PDFF observed among patients with steatosis grade 3 in those with NAFLD spectrum compared to those with inflammatory diseases.

We found that *f* decreased with higher inflammation grades. Le Bihan and Turner considered that *f* and *D** reflected the microvascular physiology [36]. At the microvascular level, recruitment and infiltration of inflammatory cells cause tissue congestion and a subsequent restriction of water molecule

diffusion. This inflammation is associated with decreased blood outflow and decreased perfusion upstream leading to congestion and edema. Hence, inflammation-mediated congestion occurring in arterioles, capillaries, and venules may lead to impaired capillary perfusion, as shown by decreased *f* measurements [37].

However, there are still knowledge gaps in the relationship between IVIM parameters and perfusion changes at the capillary level [26]. Patel et al suggested that IVIM parameters are not reflective of perfusion parameters as evaluated by dynamic contrast-enhanced MRI and may instead reflect liver parenchymal effects not assessed by the classic understanding of perfusion [38]. Under this model, the parenchymal extravasation of fluid and inflammatory cells may explain the decrease in *f* and *D** found in our study.

Our reported IVIM parameters were similar to those found by Barbieri et al who compared fitting methods in healthy patients [39] but were lower than those found by Franca et al using IVIM DWI in patients with CLD [13]. For ADC and *f*, Franca et al previously found AUCs ranging from 0.670 to 0.749 for dichotomizations between fibrosis stages or inflammation grades. Prior IVIM DWI studies in patients with

Table 3 Correlation of IVIM DWI and MRI PDFF parameters with histopathological features of liver disease. The strongest correlations were observed between perfusion fractions vs. inflammation grades and fat fractions vs. steatosis grades

		Univariate analysis		Multiple regression analysis				
		Estimated Spearman’s ρ	p value	Estimated regression coefficients	Standardized estimated regression coefficients	Standard error	p value	Adjusted R^2
Perfusion fraction (f)	Inflammation	-0.70	<0.0001	-0.022	-0.536	0.003	<0.0001	0.49
	Fibrosis	-0.46	<0.0001	-0.006	-0.263	0.002	0.002	
	Steatosis	0.35	0.001	0.004	0.133	0.002	0.075	
True diffusion coefficient (D)	Inflammation	0.103	0.33					
	Fibrosis	-0.15	0.15					
	Steatosis	-0.34	<0.001					
Pseudo-diffusion coefficient (D^*)	Inflammation	-0.27	0.010					
	Fibrosis	-0.14	0.19					
	Steatosis	0.07	0.51					
Apparent diffusion coefficient (ADC)	Inflammation	0.10	0.35					
	Fibrosis	-0.16	0.14					
	Steatosis	-0.25	0.010					
Proton density fat fraction (PDFF)	Inflammation	-0.24	0.020					
	Fibrosis	-0.20	0.054					
	Steatosis	0.88	<0.0001					

CLD focused on staging of liver fibrosis rather than grading of inflammation [7, 12, 13]. However, in an animal model of NASH, a recent study by Xie et al reported an AUC of 0.73

for distinguishing advanced inflammation from lower grades with f [20]. In our cohort of patients with CLD, we report for the first time high AUCs, ranging from 0.84 to 0.88, for

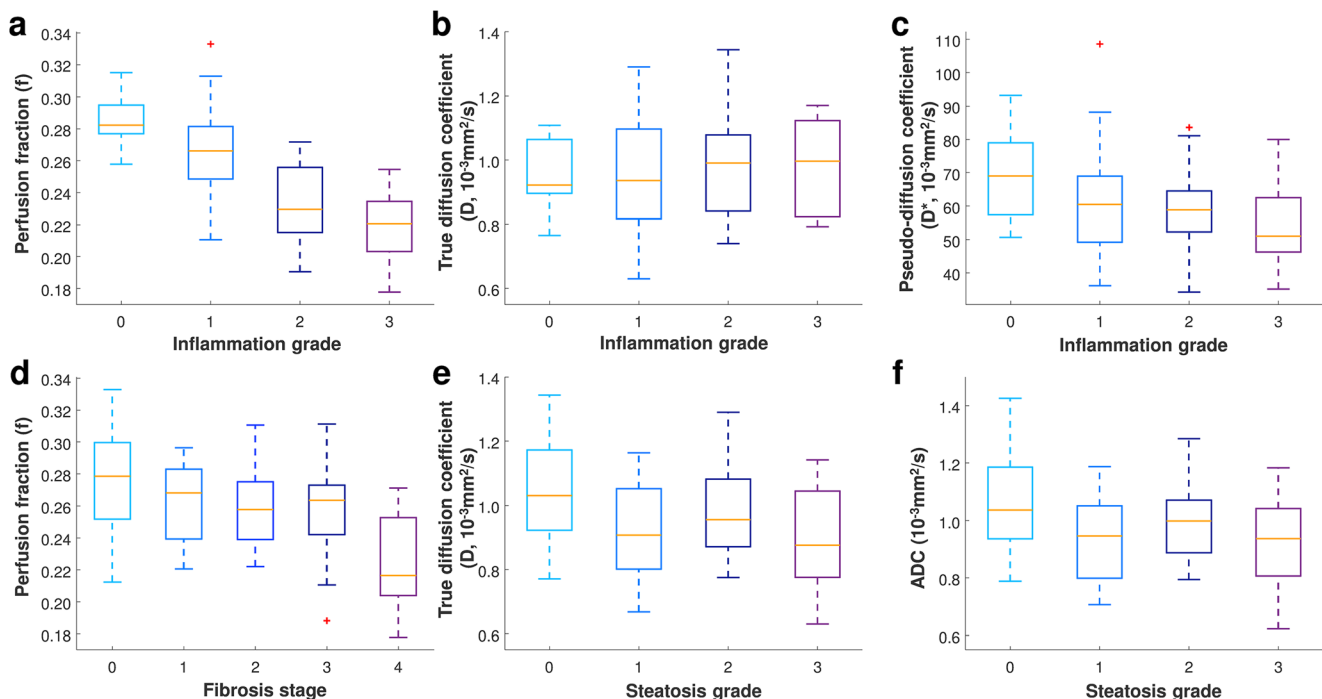


Fig. 3 Box and whisker plots of IVIM parameters— f (a), D (b), and D^* (c)—vs. inflammation grades and of index tests (d–f) significantly correlated with other histopathological features (as assessed with Spearman’s ρ rank correlation with $p < 0.01$ and omnibus Kruskal-

Wallis test with $p < 0.01$). Medians are represented by orange lines, boxes indicate first and third quartiles, whiskers indicate minimum and maximum values, and red crosses are outliers

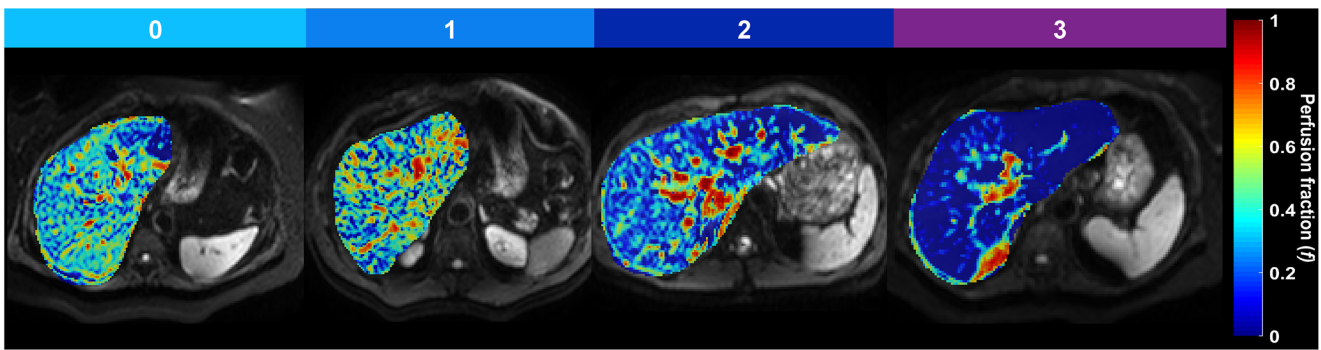


Fig. 4 Representative perfusion fraction maps in patients with different inflammation grades. Patients with inflammation grades 0, 1, 2, and 3 had perfusion fractions of 0.315, 0.310, 0.255, and 0.213, respectively

distinguishing dichotomized groups of inflammation grades suggesting that f may be used as a surrogate biomarker of inflammation. As in prior reports, we did not find that other IVIM parameters (D or D^*) could accurately classify inflammation grades.

The higher classification performance achieved in our study may be explained by the use of a fit quality-driven approach in contrast to prior studies that have mainly relied on arbitrary ROI measurements. The rationale for discarding voxels with f higher than 0.5 was to select perfusion changes at the parenchymal level, since voxels with higher f are more likely to be located in vessels or bile ducts which are difficult to distinguish from microcapillary perfusion [26]. Our analysis of a subgroup of patients who underwent manual segmentation of vessels showed good to excellent agreement with the original cohort, which supports our method for voxel selection.

Another contributor was our choice of a stringent regression success criterion (NRMSE smaller than 0.05). This likely eliminated voxels in which inconsistent diffusion or perfusion

behavior could occur across b -values due to respiratory or cardiac motion and subject to greater errors, therefore confounding parenchymal DWI signals. In a previous study, the use of a NRMSE criterion to fit the IVIM model was shown to retain voxels with higher signal-to-noise ratio [39]. This approach excluded voxels subject to noise and motion artifacts. Hence, using the two proposed criteria for selecting parenchymal voxels may have increased the reliability of IVIM parameters and improved the classification accuracy of f for grading inflammation.

In our study, f also differed between lower and higher inflammation grades in fibrosis stages F0, F1, and F4. This suggests that inflammation may have been a confounding factor in previously reported associations between fibrosis and f . However, fibrous connective tissue development within the extracellular space is linked to the progression of inflammatory activity [40]. Separating the restricted perfusion induced by the presence of extracellular matrix and collagen in fibrosis from the impaired capillary perfusion in inflammation might not be feasible solely by analyzing DWI signal variations.

Table 4 Summary of the diagnostic performance of IVIM parameters and ADC for grading histology-determined inflammation grades (95% confidence intervals in parentheses)

	Inflammation grades	AUC	Threshold	Sensitivity (%)	Specificity (%)	Accuracy (%)	PPV (%)	NPV (%)
Perfusion fraction (f)	0 vs. ≥ 1	0.84 (0.74–0.96)	0.275	88 (63–100)	82 (74–90)	82 (75–90)	32 (22–47)	99 (96–100)
	≤ 1 vs. ≥ 2	0.88 (0.82–0.95)	0.256	77 (66–89)	85 (72–95)	81 (72–88)	88 (78–95)	74 (64–84)
	≤ 2 vs. 3	0.86 (0.78–0.96)	0.242	76 (66–84)	89 (67–100)	77 (68–86)	98 (95–100)	30 (21–40)
True diffusion coefficient (D , 10^{-3} mm ² /s)	0 vs. ≥ 1	0.53 (0.33–0.71)	0.932	21 (12–32)	97 (92–100)	59 (49–69)	13 (7–20)	94 (89–100)
	≤ 1 vs. ≥ 2	0.57 (0.45–0.69)	0.989	59 (45–72)	53 (38–67)	56 (46–66)	63 (54–73)	48 (37–59)
	≤ 2 vs. ≥ 3	0.54 (0.31–0.77)	1.085	74 (64–83)	44 (12–77)	72 (62–79)	93 (88–97)	16 (5–27)
Pseudo-diffusion coefficient (D^* , 10^{-3} mm ² /s)	0 vs. ≥ 1	0.70 (0.51–0.90)	68.1	65 (20–100)	81 (71–89)	79 (69–87)	24 (9–50)	96 (89–100)
	≤ 1 vs. ≥ 2	0.60 (0.47–0.71)	68.0	32 (20–46)	90 (76–97)	59 (48–68)	81 (58–94)	49 (37–60)
	≤ 2 vs. 3	0.65 (0.43–0.85)	52.5	75 (64–83)	67 (30–100)	73 (63–82)	95 (88–100)	24 (10–41)
Apparent diffusion coefficient (ADC, 10^{-3} mm ² /s)	0 vs. ≥ 1	0.56 (0.39–0.72)	0.806	38 (13–75)	62 (52–72)	59 (50–69)	10 (2–17)	91 (87–96)
	≤ 1 vs. ≥ 2	0.56 (0.44–0.68)	1.003	55 (42–68)	58 (42–74)	56 (45–66)	64 (54–74)	48 (38–58)
	≤ 2 vs. 3	0.54 (0.33–0.75)	1.054	74 (65–84)	34 (11–67)	70 (60–79)	91 (87–96)	13 (4–25)

Data in parentheses are raw. *AUC* area under the ROC curve, *PPV* positive predictive value, *NPV* negative predictive value

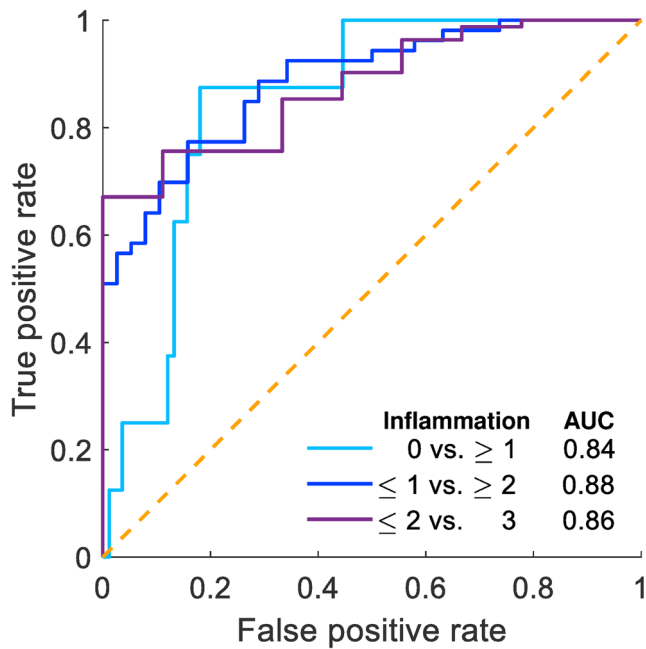


Fig. 5 Receiver operating characteristic curves of perfusion fractions for distinguishing dichotomized groups of inflammation grades

Additional findings were the higher f and PDFF values found in patients on the NAFLD spectrum compared to those with inflammatory etiologies of CLD. Considering that fat accumulation is a hallmark feature of NAFLD and NASH, the higher PDFF seen in NAFLD spectrum was expected [41]. Interestingly, this difference between stratified subgroups of CLD was not significant for f suggesting that similar perfusion changes might be observed in both liver disease subtypes.

Our study had limitations. Patients with a variety of CLD were included. Recent studies tend to produce disease-specific thresholds in homogeneous patient populations. However, the variety of etiologies in our

population allowed for assessing differences of IVIM parameters and PDFF across well-defined groups of CLD. The heterogeneity of this cohort also impacted the grading of histopathological features, since two histopathological scoring systems were used. By merging these systems, it was assumed that features of liver disease in patients with NAFLD or NASH were similar to those of inflammatory hepatitis from viral or autoimmune causes. However, considering the sufficiently large sample size, we were able to compare differences in IVIM parameters in the two subgroups of CLD. Regarding the contribution of fat to DWI signals, this was not accounted for during post-processing before applying regression to the IVIM model. However, gradient reversal and spectral presaturation (SPIR) fat suppression sequences were applied prior to the acquisition of DWI series, which reduce the confounding effect of fat [42].

In conclusion, this retrospective, cross-sectional ancillary study in patients with CLD revealed that perfusion fraction (f) was the only IVIM parameter that decreased with inflammation and provided moderate to good diagnostic performance for grading inflammation. The correlation between inflammation and f was confounded by the presence of fibrosis. In subgroups of liver disease with inflammatory or fatty causes, f did not significantly differ within any inflammation grades, while PDFF within advanced steatosis grade was higher in patients with NAFLD than in those with inflammatory liver diseases. Prospective studies assessing IVIM DWI sequences may provide information on inflammatory activity and complement the use of MR elastography for staging liver fibrosis and PDFF for grading liver steatosis. Validation studies in cohorts of patients with specific causes of CLD will be required to develop a noninvasive one-stop-shop alternative to liver biopsy.

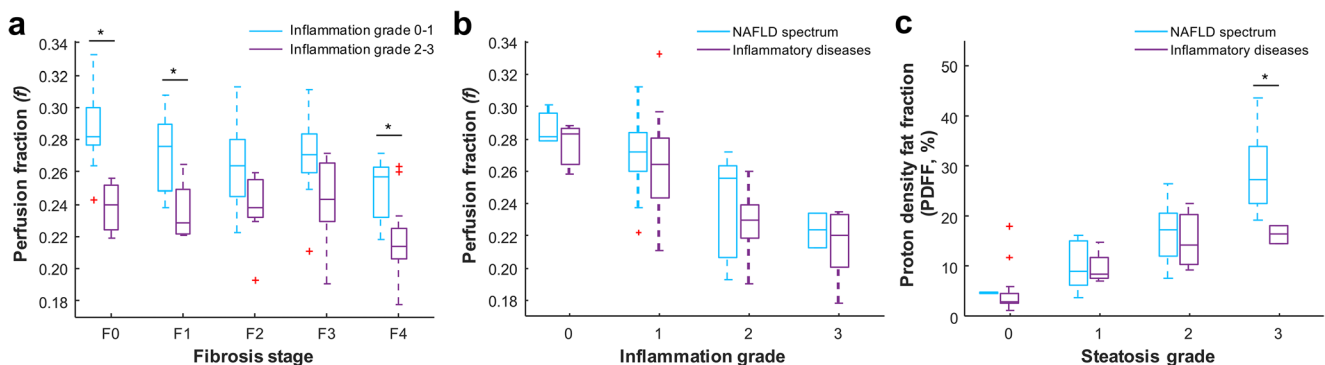


Fig. 6 Box and whisker plots of perfusion fractions across fibrosis stages (a) in dichotomized groups of patients with lower grades (0–1) from higher grades (2–3) of inflammation, perfusion fractions (b) across inflammation grades, and proton density fat fractions (c) across steatosis

grades in dichotomized groups of patients with inflammatory liver disease (HBV, HCV, or AIH) and in patients with fatty liver disease (NAFLD or NASH) ($*p < 0.01$)

Acknowledgments We thank Mr. Walid El Abyad, Mrs. Catherine Huet, and Mrs. Assia Belblidia for their assistance in patient enrollment, acquisition, and post-processing of MRI data.

Funding This study has received funding by grants from the Canadian Institutes of Health Research (CIHR)-Institute of Nutrition, Metabolism and Diabetes (INMD) (CIHR-INMD #273738 and #301520) and Fonds de recherche du Québec en Santé (FRQS) and Fondation de l'association des radiologistes du Québec (FARQ) Clinical Research Scholarship – Junior 1 and 2 Salary Award (FRQS-FARQ #26993 and #34939) to An Tang. Junior 1 Salary Award from FRQS (#27127) and research salary from McGill University to Giada Sebastiani. Junior 1 Salary Award from FRQS to Marie-Pierre Sylvestre (#34875).

Compliance with ethical standards

Guarantor The scientific guarantor of this publication is Dr. An Tang.

Conflict of interest The authors of this manuscript declare relationships with the following companies: Philips Healthcare Canada (Guillaume Gilbert is an employee of Philips Healthcare Canada).

Statistics and biometry Dr. Marie-Pierre Sylvestre is one of the authors and has significant statistical expertise.

Informed consent Written informed consent was obtained from all subjects in this study.

Ethical approval Institutional Review Board approval was obtained for the two participating institutions, Centre hospitalier de l'Université de Montréal (CHUM) and McGill University Health Centre (MUHC).

Study subjects or cohorts overlap The patients included in this ancillary study represent a subset of 91 patients from the cohort in the prior report [23]

Methodology

- retrospective
- cross-sectional study
- multicenter study

References

1. Younossi ZM, Blissett D, Blissett R et al (2016) The economic and clinical burden of nonalcoholic fatty liver disease in the United States and Europe. *Hepatology* 64:1577–1586
2. Bedossa P (2017) Pathology of non-alcoholic fatty liver disease. *Liver Int* 37(Suppl 1):85–89
3. Yin M, Glaser KJ, Manduca A et al (2017) Distinguishing between hepatic inflammation and fibrosis with MR elastography. *Radiology* 284:694–705
4. Argo CK, Northup PG, Al-Osaimi AM, Caldwell SH (2009) Systematic review of risk factors for fibrosis progression in non-alcoholic steatohepatitis. *J Hepatol* 51:371–379
5. Poynard T, Mathurin P, Lai CL et al (2003) A comparison of fibrosis progression in chronic liver diseases. *J Hepatol* 38:257–265
6. Zhang B, Liang L, Dong Y et al (2016) Intravoxel incoherent motion MR imaging for staging of hepatic fibrosis. *PLoS One* 11: e0147789
7. Jiang H, Chen J, Gao R, Huang Z, Wu M, Song B (2017) Liver fibrosis staging with diffusion-weighted imaging: a systematic review and meta-analysis. *Abdom Radiol (NY)* 42:490–501
8. Lewin M, Poujol-Robert A, Boelle PY et al (2007) Diffusion-weighted magnetic resonance imaging for the assessment of fibrosis in chronic hepatitis C. *Hepatology* 46:658–665
9. Taouli B, Chouli M, Martin AJ, Qayyum A, Coakley FV, Vilgrain V (2008) Chronic hepatitis: role of diffusion-weighted imaging and diffusion tensor imaging for the diagnosis of liver fibrosis and inflammation. *J Magn Reson Imaging* 28:89–95
10. Taouli B, Tolia AJ, Losada M et al (2007) Diffusion-weighted MRI for quantification of liver fibrosis: preliminary experience. *AJR Am J Roentgenol* 189:799–806
11. Sandrasegaran K, Territo P, Elkady RM et al (2018) Does intravoxel incoherent motion reliably stage hepatic fibrosis, steatosis, and inflammation? *Abdom Radiol (NY)* 43:600–606
12. Leitao HS, Doblas S, Garteiser P et al (2017) Hepatic fibrosis, inflammation, and steatosis: influence on the MR viscoelastic and diffusion parameters in patients with chronic liver disease. *Radiology* 283:98–107
13. Franca M, Marti-Bonmati L, Alberich-Bayarri A et al (2017) Evaluation of fibrosis and inflammation in diffuse liver diseases using intravoxel incoherent motion diffusion-weighted MR imaging. *Abdom Radiol (NY)* 42:468–477
14. Le Bihan D, Breton E, Lallemand D, Aubin ML, Vignaud J, Laval-Jeantet M (1988) Separation of diffusion and perfusion in intravoxel incoherent motion MR imaging. *Radiology* 168: 497–505
15. Murphy P, Hooker J, Ang B et al (2015) Associations between histologic features of nonalcoholic fatty liver disease (NAFLD) and quantitative diffusion-weighted MRI measurements in adults. *J Magn Reson Imaging* 41:1629–1638
16. Manning P, Murphy P, Wang K et al (2017) Liver histology and diffusion-weighted MRI in children with nonalcoholic fatty liver disease: a MAGNET study. *J Magn Reson Imaging* 46:1149–1158
17. Huang H, Che-Nordin N, Wang LF et al (2019) High performance of intravoxel incoherent motion diffusion MRI in detecting viral hepatitis-b induced liver fibrosis. *Ann Transl Med* 7:39
18. Lu PX, Huang H, Yuan J et al (2014) Decreases in molecular diffusion, perfusion fraction and perfusion-related diffusion in fibrotic livers: a prospective clinical intravoxel incoherent motion MR imaging study. *PLoS One* 9:e113846
19. Fujimoto K, Tonan T, Azuma S et al (2011) Evaluation of the mean and entropy of apparent diffusion coefficient values in chronic hepatitis C: correlation with pathologic fibrosis stage and inflammatory activity grade. *Radiology* 258:739–748
20. Xie Y, Zhang H, Jin C et al (2018) Gd-EOB-DTPA-enhanced T1rho imaging vs diffusion metrics for assessment liver inflammation and early stage fibrosis of nonalcoholic steatohepatitis in rabbits. *Magn Reson Imaging* 48:34–41
21. Joo I, Lee JM, Yoon JH, Jang JJ, Han JK, Choi BI (2014) Nonalcoholic fatty liver disease: intravoxel incoherent motion diffusion-weighted MR imaging—an experimental study in a rabbit model. *Radiology* 270:131–140
22. Younossi ZM, Koenig AB, Abdelatif D, Fazel Y, Henry L, Wymer M (2016) Global epidemiology of nonalcoholic fatty liver disease—meta-analytic assessment of prevalence, incidence, and outcomes. *Hepatology* 64:73–84
23. Lefebvre T, Wartelle-Bladou C, Wong P et al (2019) Prospective comparison of transient, point shear wave, and magnetic resonance elastography for staging liver fibrosis. *Eur Radiol* 29:6477–6488
24. Hansmann J, Hernando D, Reeder SB (2013) Fat confounds the observed apparent diffusion coefficient in patients with hepatic steatosis. *Magn Reson Med* 69:545–552

25. Gomori JM, Holland GA, Grossman RI, Gefter WB, Lenkinski RE (1988) Fat suppression by section-select gradient reversal on spin-echo MR imaging. Work in progress. *Radiology* 168:493–495
26. Iima M, Le Bihan D (2016) Clinical intravoxel incoherent motion and diffusion MR imaging: past, present, and future. *Radiology* 278:13–32
27. Taouli B, Beer AJ, Chenevert T et al (2016) Diffusion-weighted imaging outside the brain: consensus statement from an ISMRM-sponsored workshop. *J Magn Reson Imaging* 44:521–540
28. Benovoy M, Jacobs M, Cheriet F, Dahdah N, Arai AE, Hsu LY (2017) Robust universal nonrigid motion correction framework for first-pass cardiac MR perfusion imaging. *J Magn Reson Imaging* 46:1060–1072
29. Yokoo T, Bydder M, Hamilton G et al (2009) Nonalcoholic fatty liver disease: diagnostic and fat-grading accuracy of low-flip-angle multiecho gradient-recalled-echo MR imaging at 1.5 T. *Radiology* 251:67–76
30. Bydder M, Yokoo T, Yu H, Carl M, Reeder SB, Sirlin CB (2011) Constraining the initial phase in water-fat separation. *Magn Reson Imaging* 29:216–221
31. Kleiner DE, Brunt EM, Van Natta M et al (2005) Design and validation of a histological scoring system for nonalcoholic fatty liver disease. *Hepatology* 41:1313–1321
32. Bedossa P, Poynard T (1996) An algorithm for the grading of activity in chronic hepatitis C. The METAVIR Cooperative Study Group. *Hepatology* 24:289–293
33. Shrout PE, Fleiss JL (1979) Intraclass correlations: uses in assessing rater reliability. *Psychol Bull* 86:420–428
34. Schober P, Boer C, Schwarte LA (2018) Correlation coefficients: appropriate use and interpretation. *Anesth Analg* 126:1763–1768
35. DeLong ER, DeLong DM, Clarke-Pearson DL (1988) Comparing the areas under two or more correlated receiver operating characteristic curves: a nonparametric approach. *Biometrics* 44:837–845
36. Le Bihan D, Turner R (1992) The capillary network: a link between IVIM and classical perfusion. *Magn Reson Med* 27:171–178
37. Granger DN, Senchenkova E (2010) Inflammation and the microcirculation. Morgan & Claypool Life Sciences. San Rafael, CA
38. Patel J, Sigmund EE, Rusinek H, Oei M, Babb JS, Taouli B (2010) Diagnosis of cirrhosis with intravoxel incoherent motion diffusion MRI and dynamic contrast-enhanced MRI alone and in combination: preliminary experience. *J Magn Reson Imaging* 31:589–600
39. Barbieri S, Gurney-Champion OJ, Klaassen R, Thoeny HC (2020) Deep learning how to fit an intravoxel incoherent motion model to diffusion-weighted MRI. *Magn Reson Med* 83:312–321
40. Neubauer K, Saile B, Ramadori G (2001) Liver fibrosis and altered matrix synthesis. *Can J Gastroenterol* 15:870205
41. Diehl AM, Day C (2017) Cause, pathogenesis, and treatment of nonalcoholic steatohepatitis. *N Engl J Med* 377:2063–2072
42. Leitao HS, Doblaz S, d'Assignies G et al (2013) Fat deposition decreases diffusion parameters at MRI: a study in phantoms and patients with liver steatosis. *Eur Radiol* 23:461–467

Publisher's note Springer Nature remains neutral with regard to jurisdictional claims in published maps and institutional affiliations.